Low grazing angle reflection and the shear-wave resonance over a layer of elastic–solids sediment*

XIE Jinhuai[1, 2, 3], ZHANG Haigang[1, 2, 3, *], CAO Dejin[1, 2, 3]

1. National Key Laboratory of Underwater Acoustic Technology, Harbin Engineering University, Harbin 150001, China
2. Key Laboratory of Marine Information Acquisition and Security, Ministry of Industry and Information Technology, Harbin Engineering University, Harbin 150001, China
3. College of Underwater Acoustic Engineering, Harbin Engineering University, Harbin 150001, China

Abstract

The low-grazing-angle reflection from an elastic sediment seabed exhibits singularly enhanced frequency characteristics, which significantly influence long-range sound propagation in shallow water. To study the influence of the elastic sedimentary seabed environment on long-range sound propagation in shallow water, we conducted a joint seabed and waveguide sound propagation experiment in the Dongsha area of the South China Sea. The experiment recorded the simultaneous occurrence of seabed resonance and the sound siphon effect for the first time. Notably, this effect differs from the sound siphon effect observed in low-sound-speed seabed environments, as it exhibits smaller frequency intervals. By analyzing the low-grazing-angle reflection characteristics of the elastic seabed, we derived a theoretical model for the resonance frequencies of shear waves in elastic sediment layers under small grazing angles and investigated their impact on long-range sound propagation. The results demonstrate that under an elastic seabed model, the low-grazing-angle reflection modulated by shear waves induces resonance at specific frequencies within the sediment layer. This traps acoustic energy in the seabed, leading to the sound siphon effect. Furthermore, we analyzed the sensitivity and coupling of key parameters related to shear-wave resonance frequencies. Based on these findings, we developed an inversion strategy that integrates seabed and waveguide observations to estimate geo-acoustic parameters of the experimental area. The inversion results validate the mechanism through which the elastic seabed model contributes to the sound siphon effect in the water column.

---

* The paper is an English translated version of the original Chinese paper published in Acta Physica Sinica. Please cite the paper as: XIE Jinhuai, ZHANG Haigang, CAO Dejin, **Low grazing angle reflection and shear-wave resonance on elastic-solid sediment**. *Acta Phys. Sin.*, 2025, 74(16): 164301. doi: 10.7498/aps.74.20250656

Keywords: low grazing angle reflection; shear wave resonance; sound siphon effect

PACS: 43.30.Ma; 43.30.+m; 43.30.Pc
doi: 10.7498/aps.74.20250656
cstr: 32037.14.aps.74.20250656

1. Introduction

The influence of the reflection characteristics of seafloor sediments on the long-range sound propagation in shallow water is an important subject in underwater acoustics[1]. Based on differences in the geoacoustic characteristics of seafloor sediments, various acoustic models can be established for approximate descriptions. When the seafloor sediment consists of an unconsolidated mixture of sand, clay, or silt with a sufficiently low shear modulus, the acoustic medium of the sediment can be reasonably approximated as a fluid. However, in some shallow sea areas with active marine dynamic processes, where sediment migration is active, and the unconsolidated sediment layer is thin, the shear effect of the seafloor medium will significantly affect the acoustic propagation characteristics of the overlying water[2]. To accurately represent the acoustic characteristics of the actual seabed, the shear effect in the ocean sediment becomes an important factor in the interaction between the seabed and the[3], and the seabed sediment can be described as an elastic medium.

Due to the consideration of shear effects, the acoustic reflection characteristics of an elastic seabed are often more complex than those of a fluid seabed environment, which leads to the acoustic propagation characteristics in water being a research field of concern[4,5]. For example, when Duncan et al[2]. studied low-frequency sound propagation in the Australian continental shelf area, they found that the sound propagation loss was relatively low in a narrow frequency band slightly higher than the critical frequency of the low-order mode when the seabed consisted of soft, elastic limestone; When Vidmar[6] and Xie[7] analyzed the intensity of particle velocity received by the boundary, they found that the shear effect of submarine sediments would lead to a strong increase in the vertical displacement of particle vibration velocity; As well as resonance effects of the interaction between acoustic waves and elastic seabeds[8], such as resonances associated with shear-velocity gradients and marine seismic noise in upper sediments[9], and the resonance of longitudinal wave between acoustic wave and soft marine sediments[10,11].

In 1980, Hastrup[12] first predicted through numerical simulation that a specific frequency with poor propagation effect would be generated due to the small grazing reflection loss anomaly of the low-sound sediment seabed. In recent years, acoustic studies of low-sound-velocity sediments have become an increasingly important research field due to measurement

experiments[13–15] in the seabed environment of low sound velocity sediments[16]. In 2019, Li Mengzhu et al.[17] proposed an acoustic inversion method of seafloor parameters for low sound velocity sediments based on the phenomenon that the acoustic propagation loss of different frequencies in shallow water increases periodically. In 2024, Zhou et al[18], combined with the results of the Yellow Sea experiment in 2002, made a thorough study of the phenomenon involving an abnormal increase in underwater propagation loss caused by small grazing angle reflection from the seabed of low acoustic velocity sediments, and named the phenomenon "sound siphon effect" for the first time. Its essence is that the acoustic energy at a given frequency is confined by the seafloor sediments due to the small grazing angle reflection anomaly of the seafloor with low acoustic velocity sediments, which leads to the abnormal increase of the corresponding frequency propagation loss in water. Similar acoustic propagation characteristics have been found in elastic seafloor environments. In 1990, Hughes et al.[19] observed high transmission loss in the 10-100 Hz frequency band in shallow water acoustic propagation experiments with bedrock covered by a thin sediment layer, and verified that the observed high transmission loss is related to shear wave resonance in the sediment layer. In 2021, Hovem et al.[20] discussed the influence of a thin sediment layer on low-frequency and long-range propagation from the theoretical and experimental point of view. Their work demonstrated that when a hard-rock substrate is overlain by a soft elastic layer, shear wave resonance may occur, resulting in many high transmission losses at very narrow frequencies. Clearly, the high-transmission-loss features in an elastic sedimentary seabed resemble the acoustic siphon effect in low-sound-velocity seabeds, but their formation environment, mechanism, and characteristics are obviously different. To date, reports on similar acoustic propagation effects arising from elastic sedimentary seabeds remain few, and the corresponding joint observation experimental data are also relatively scarce.

In 2021, an acoustic propagation experiment was carried out in the continental slope area of the northeastern South China Sea, in which the ocean bottom seismometer (OBS) and the vertical linear array (VLA) were used to simultaneously measure the acoustic propagation in the seabed and water. Interestingly, the OBS particle velocity signals exhibit distinct peaks in their power spectra (indicating resonance), and the VLA observed siphon features with a smaller frequency interval than those typical of low-sound-speed seabed sound siphons. Therefore, to study the modulation of the measured acoustic phenomena by the seafloor, the resonance theory between the elastic seafloor and the shear wave is derived under the condition of a low grazing angle of the elastic seafloor, which is used to qualitatively explain the main characteristics of the observed results. We aim to reveal the physical mechanism behind the seabed resonance and acoustic siphon effect observed in our experiment, and to provide new insights into the influence of shallow elastic bottom on underwater sound propagation.

Section 2 describes the experiments on which this work is based, as well as the bottom resonance phenomenon observed with OBS and the acoustic siphon effect observed with the vertical array. In section 3, the low-grazing angle reflection characteristics of the elastic bottom are analyzed first, and then the analytical expression of the shear wave resonance frequency on the elastic bottom is derived theoretically, and the relationship between the low-grazing angle reflection of the elastic sediment bottom and the shear wave resonance is revealed, and the influence of the bottom reflection characteristics on the underwater sound propagation is expounded. In section 4, the sensitivity of the expression of shear wave resonance frequency to acoustic attenuation and the coupling relationship between the related parameters are analyzed, and a geoacoustic parameter inversion method combining the seafloor and waveguide observation information is further proposed to invert the seafloor geoacoustic parameters in the experimental area, and the inversion results are used to verify the mechanism of acoustic siphon by the elastic sediment seafloor.

2. Experimental data

2.1 Experimental Introduction

In July 2021, a sound propagation experiment[21] was carried out in the Dongsha sea area in the northeast of the South China Sea. The terrain environment of the experiment and the relative position of the receiving system and the sound source are shown in the Fig. 1(a). The vertical linear array (VLA) was deployed at station O_2. It consisted of 32 elements spaced 2 m apart, and operated at a depth of 200-264 m. The sensitivity of the receiving system is -196 dB, the amplification is 40 dB, and the sampling rate is 10 kHz, and was used to acquire underwater acoustic signals. The OBS is deployed on the seafloor at the O_3 point with a sampling rate of 100 SPS. The OBS three-component vector sensor is used to receive seafloor vibration information.

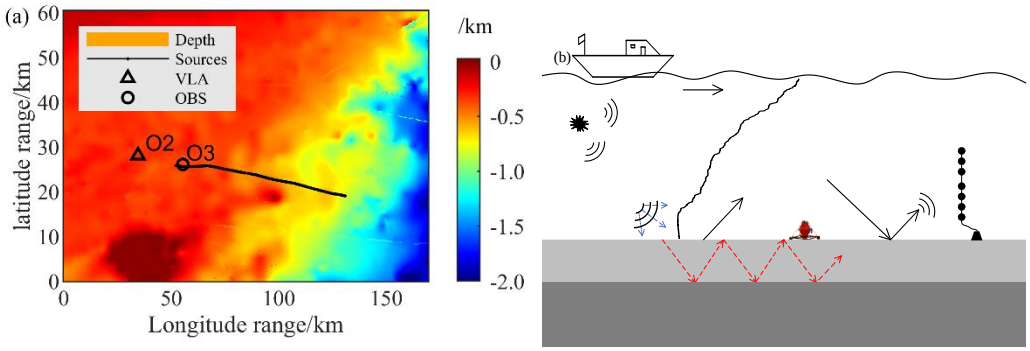

Figure 1. Experimental environment and schematic diagram: (a) Topography of sound propagation experiment area and location of receiver; (b) schematic diagram of synchronous measurement experiment of sound propagation in seabed and waveguide.

During the sound propagation experiment, the sound source ship dropped the sound source from a long range to the direction of the O_2 point along the survey line (black dot line) shown in Fig. 1(a). During the voyage, one explosive sound source was dropped every 8 minutes (the horizontal distance interval was about 1.56 km). A total of 49 explosive sound sources were dropped within a range of 19.23 — 94.28 km from the VLA. The explosion depth of the sound source was 100 m, with a real-depth error of less than ±3%. Within the range of the sound source trajectory, the seafloor topography in the area 19.23-31.14 km from the VLA is relatively flat, with a water depth of about 340 m. Therefore, in areas with relatively flat terrain, the joint seabed-water-column measurement concept is illustrated in Fig. 1(b). The sound-speed profile shown was obtained using a CTD system at the O_2 during the experiment.

In September 2021, a multi-channel seismic exploration experiment was carried out in the adjacent area of the experimental sea area, and the geological profile shown in Fig. 2 was obtained by inversion of these data. The layered structure of the seafloor in the experimental area is obvious, and the compressional wave velocity of the top sediment layer is 1637~1673 m/s, indicating a typical high-speed (or "hypersonic") seabed[22]. Historical data also show that the seafloor surface sediments in the experimental area are mainly composed of silty sand and clayey silt[23].

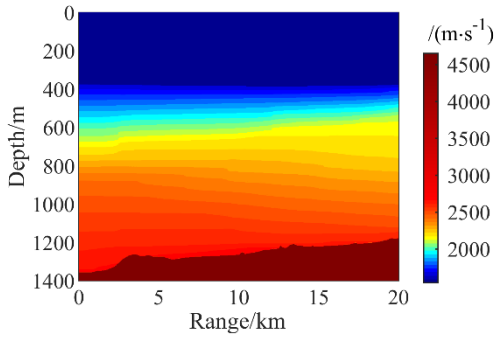

Figure 2. Seabed profile inversion using multichannel seismic data in adjacent areas.

2.2 Submarine resonance phenomenon

When using an OBS to measure seafloor sediments, it is easy to observe the resonance phenomenon on the seafloor from the particle velocity signal because the three-component vibration velocity channels are more sensitive to seafloor vibrations. For example, in 1993, Godin and Chapman[9] observed pronounced resonances between ambient noise and shear waves on the horizontal and vertical geophones of an OBS. Similarly, resonances between soft sediment and compressional waves were observed on the three-component vector sensors of an ocean bottom cable (OBC) during a shear wave survey experiment in 2007[10]. Therefore, to analyze the seafloor vibration information caused by the explosion sound source observed by the South China Sea experimental OBS, the frequency spectra of the particle velocity signals received by the OBS three-component vector sensor were calculated. The Fig. 3(a) gives the normalized spectrum of

the sound source at a distance of 16.46 km from the OBS. The spectra show significant differences among the three component vector sensor signals, which are caused by the uncertainty in the spatial direction of a single vector sensor. However, there is a common feature that two distinct spectral peaks are present at 11.8 and 37 Hz, as indicated by the red circles in Fig. 3(a), where the radial component of the horizontal velocity shows the most prominent peak at 11.8 Hz.

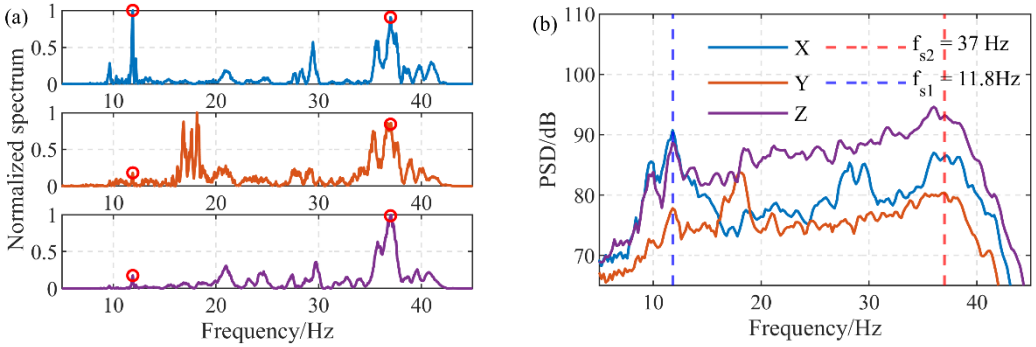

Figure 3. Particle velocity signal measured by OBS: (a) Normalized spectrum of a sound source and OBS at a distance of 16.46 km, normalized spectra of the radial (top) and cross-range (middle) components of the horizontal particle velocity, as well as vertical particle velocity (bottom); (b) the power spectral density averages 15 explosion sound source signals within the 2.7–24.8 km range from the OBS.

Compared with the potential variability of a single sound source, the average result of multiple sound sources can better reflect the statistical characteristics of the received signal. Therefore, the average power spectral density (PSD) of 15 explosive source signals at ranges of 2.7-24.8 km from the OBS was calculated, and the results are shown in Fig. 3(b). Although the PSD curves of the three particle velocity components show different energy levels in the 5-45 Hz frequency band, the spectral peak characteristics at the frequencies of 11. 8 and 37 Hz are still obvious. The sharp peaks at 11.8 and 37 Hz can be interpreted as seabed resonances arising from the experimental acoustic propagation conditions. Unlike the vertical-polarization shear-wave resonance frequency interval[9] ($\Delta f = 1.11 \pm 0.04$ Hz) excited by infrasonic seismic ambient noise in the Scottish Continental Shelf experiment and the longitudinal wave resonance frequency interval[10] ($\Delta f > 85$Hz) of the soft sediment of the shear wave survey experiment, the experimentally measured resonance frequency interval $\Delta f \approx 26$Hz .

2.3 Acoustic siphon phenomenon

The acoustic siphon effect occurs when small-grazing-angle reflection anomalies and resonantly excited leaky modes occur simultaneously in the subsea layer at low acoustic speeds[18]. In the experiment, both OBS and VLA were used to receive the explosive source signals, enabling simultaneous observation of seabed resonance phenomena and siphon characteristics in the waveguide sound propagation. The Fig. 4(a) shows the PSD distribution in the 50-300 Hz frequency band for sources at distances of 19.2-50.0 km from the VLA. Fig. 4(a) shows that the

PSD exhibits stable bright and dark fringe patterns in the frequency domain, which is different from the feature of shallow water interference structure changing with distance. At ranges less than 30 km and greater than 40 km, the PSD bright and dark stripes remain stable with distance, and have a stable frequency interval. However, in the 30-40 km range, the patterns show an obvious shift with distance, attributed to significant seabed topographic variations in the 30-40 km range [21].

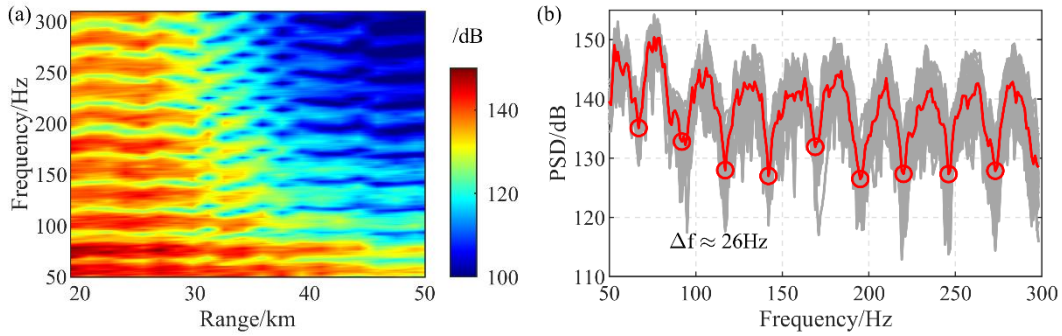

Figure 4. Explosion sound signal measured by VLA: (a) PSD within the range of 19.2–50.0 km from the sound source and VLA, where the PSD of each distance is the average result of all array metadata of the VLA; (b) PSD with a distance of 20.8 km between the sound source and the VLA.

To more intuitively describe the frequency characteristics of the received signals, the PSD curve for a source-VLA distance of 20.8 km is shown in Fig. 4(b), where gray curves represent results from individual array elements and the red curve shows the average result. The PSD curve shows $\Delta f = 26\text{Hz}$ periodic energy dips, such as at the frequencies indicated by red circles in Fig. 4(b). Comparing this phenomenon with the acoustic siphon effect caused by small-grazing-angle (<5°) reflection from low-sound-speed fluid seabeds reveals that: 1) For reasonable seabed parameter ranges, the acoustic siphon frequency interval on low-sound-speed seabeds is typically on the order of hundreds of hertz, for example, Zhou et al. [18] observed a 512 Hz interval, whereas the Dongsha experiment observed an interval of 26Hz; 2) Multichannel seismic exploration results indicate that the seabed in the experimental area is a high-sound-speed seabed. From the measured sound-speed profile, the minimum grazing angle for signals received by the VLA (deployed at 200-264 m depth) from sources at 100 m depth can be calculated, which differs from the low-grazing-angle (<5°) reflection singularities characteristic of low-sound-speed seabeds.

Combining this with the peak frequencies in the vibration velocity spectra measured by OBS shows that both the measured seabed resonance and acoustic siphon frequency intervals are approximately 26 Hz. Fig. 5 shows PSD curves for three sources received by the VLA at different distances in the frequency band of 20-150 Hz, revealing an energy dip at 37 Hz that coincides with the particle velocity peak frequency observed on the seabed. These combined seabed and waveguide measurements visually demonstrate that the underwater acoustic siphon effect is related to acoustic resonance within the seabed sediment layer.

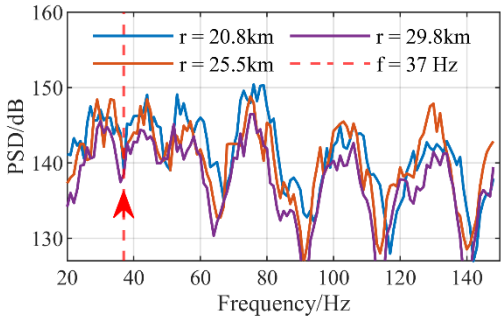

Figure 5. The PSD of the 20–150 Hz frequency band has an energy depression at 37 Hz.

Compared with previous studies of the acoustic siphon effect in low-sound-velocity seabeds[17,18], the approximately 26 Hz interval siphon effect cannot be explained by longitudinal wave resonance in low-sound-velocity seabeds, given reasonable sediment layer compressional wave velocities (>1400 m/s). Moreover, multichannel seismic inversion results and historical data indicate the experimental area has a typical high-speed seabed. Considering that shear wave velocities in elastic sedimentary layers are generally lower than the sound speed in water, it can be inferred that resonance between the sedimentary layer and shear waves is responsible for the acoustic siphon effect with small frequency spacing.

3. Low grazing angle reflection and shear wave resonance on elastic seafloor

To theoretically verify the relationship between low-grazing-angle reflection and shear-wave resonance on elastic sedimentary seabeds, and to analyze the influence of elastic seabed geoacoustic model on sound propagation in water. In this section, the reflection characteristics of elastic sediment seabed, the formation conditions of shear wave resonance frequency, and the acoustic propagation characteristics in the corresponding environment are studied.

3.1 Low grazing angle reflection characteristics of the elastic sediment seafloor

Table 1. Acoustic parameters of low sound velocity sediment seabed.

Acoustic Parameters	Compression wave Velocity/(m·s^{-1})	Thickness/(m)	Density/(g·cm^{-3}).	Compression wave attenuation/(dB·λ^{-1})
Water	1499	100	1.0	0
Sedimentary	1465	15	1.6	0.1
Basement	1650	—	1.9	0.2

Considering the layered elastic seabed model shown in Fig. 6, the sediment parameters within the elastic layer are assumed constant, while both the overlying water (fluid half-space) and underlying basement (elastic half-space) are homogeneous and semi-infinite. Where c_1 and ρ_1 are the sound speed and density in water; the compressional wave speed is c_{p2}, shear wave speed is c_{s2}, thickness is h, and density is ρ_2, with compressional wave attenuation α_{p2} and shear wave attenuation α_{s2} in the sedimentary layer; the basement has compressional wave speed c_{p3}, shear wave speed c_{s3}, and density ρ_3, with compressional wave attenuation α_{p3} and shear wave attenuation α_{s3}. θ is the grazing angle in water, θ_{p} and θ_{s} are the refraction angles for compressional and shear waves, respectively. Referring to small-grazing-angle reflection from low-sound-speed sediment bottoms, we assume the shear wave speeds satisfy $c_{\mathrm{s2}} < c_1 < c_{\mathrm{s3}}$, and the compressional wave speeds satisfy $c_1 < c_{\mathrm{p2}} < c_{\mathrm{p3}}$.

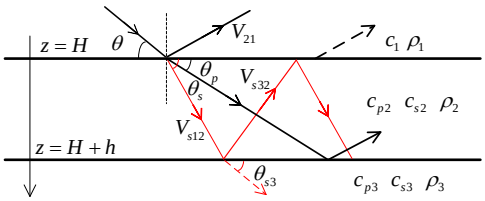

Figure 6. Submarine geo-acoustic model of elastic sedimentary layer.

Fig. 7 shows the frequency dependence of reflection loss for low-sound-speed sediment beds, elastic sediment beds, and high-sound-speed fluid sediment beds. Fig. 7(a) shows that low-grazing-angle reflection loss exhibits singular maxima at equal frequency intervals for low-sound-speed sedimentary bottoms. The siphon effect observed in the 2002 Yellow Sea experiment has been explained by these small-grazing-angle reflection characteristics[18]. For elastic sedimentary bottoms (Fig. 7(b)), the small-grazing-angle reflection loss singularities are similar to those for fluid low-sound-speed bottoms. However, the frequency interval is smaller, with seven siphon frequencies in the 50-200 Hz band and an interval of 19.5 Hz, whereas the acoustic siphon interval for low-sound-speed sediments in Fig. 7(a) is 230 Hz. Additionally, the grazing angle range over which the reflection loss singularities occur for the elastic sediment layer is $\theta < \arccos\left(c_1/c_{\mathrm{p2}}\right)$. Fig. 7(c) shows reflection loss for a high-speed fluid sediment bottom with the same compressional wave speed as the elastic bottom. Since shear waves with speeds lower than the water sound speed are not considered, sound waves at angles below the compressional wave critical angle cannot penetrate into the sediment. In this case, low-grazing-angle reflection loss is frequency-independent, demonstrating that shear waves modulate the low-grazing-angle reflection features.

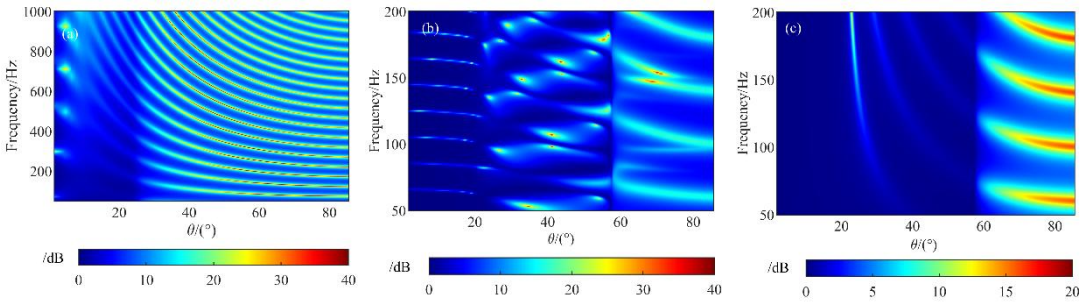

Figure 7. Relationship between seabed reflection loss and frequency. Porter's Bounce program calculates the reflection loss: (a) The geo-acoustic parameters of the seabed of low-velocity sediments are shown in Table 1; (b) geo-acoustic parameters of elastic sedimentary seabed are shown in Table 2; (c) all the parameters except the shear wave parameters in Table 2 are used in the high-velocity liquid deposition seabed.

3.2 Shear wave resonance in elastic deposits

Further analyzing the relationship between low-grazing-angle reflection from elastic sediment bottoms and seabed shear-wave resonance, plane wave reflection from the water-elastic sediment interface can be approximated as the water-elastic semi-infinite case, neglecting reflections from the $z = H + h$ boundary, yields the reflection coefficient:

$$V = \frac{Z_{\mathrm{p}} \cos^2 2\theta_{\mathrm{s}} + Z_{\mathrm{s}} \cos^2 2\theta_{\mathrm{s}} - Z}{Z_{\mathrm{p}} \cos^2 2\theta_{\mathrm{s}} + Z_{\mathrm{s}} \cos^2 2\theta_{\mathrm{s}} + Z} \tag{1}$$

Where Z_{p} and Z_{s} are the compressional and shear wave impedances in the elastic medium, and Z is the wave impedance in water. Considering $c_{\mathrm{s2}} < c_1 < c_{\mathrm{p2}}$, when the grazing angle satisfies $\theta < \arccos\left(c_1 / c_{\mathrm{p2}}\right)$, the reflection coefficient becomes:

$$V = \frac{Z_{\mathrm{s}} \cos^2 2\theta_{\mathrm{s}} - Z - i\left|Z_{\mathrm{p}}\right| \cos^2 2\theta_{\mathrm{s}}}{Z_{\mathrm{s}} \cos^2 2\theta_{\mathrm{s}} + Z - i\left|Z_{\mathrm{p}}\right| \cos^2 2\theta_{\mathrm{s}}} \tag{2}$$

In this case, the compressional wave in the elastic deposit becomes inhomogeneous, while the shear wave remains a standard plane wave. This implies that low-grazing-angle reflection from elastic sedimentary bottoms can be simplified to a scenario involving only shear wave interactions at the bottom, and that long-range acoustic propagation in shallow water is typically dominated by low-order normal modes at low grazing angles. Therefore, when discussing shear-wave resonance on elastic sedimentary bottoms, the analysis of bottom reflection characteristics can be limited to the $\theta < \arccos\left(c_1 / c_{\mathrm{p2}}\right)$ grazing angle range.

Under low-grazing-angle conditions $\theta < \arccos\left(c_1 / c_{\mathrm{p2}}\right)$, resonance occurs when shear waves in the $H < z < H + h$ layer waveguide satisfy condition Eq. (3):

$$V_{s12}V_{s32}\exp\left(2i\omega h\sqrt{c_{s2}^{-2}-u^{-2}}\right)=1 \tag{3}$$

where the reflection coefficients V_{s12} and V_{s32} have distinct meanings, V_{s12} represents the shear wave reflection coefficient at the upper boundary of the sedimentary layer, and V_{s32} represents the shear wave reflection coefficient at the lower boundary; u is the shear wave phase velocity and $\omega=2\pi f$ is the angular frequency. According to beam ray normal mode theory, Eq. (3)[27] can be expressed as:

$$\phi_{s12}+\phi_{s32}+2\omega h\sqrt{c_{s2}^{-2}-u^{-2}}=2(n-1)\pi, \qquad n=1,2,3,\cdots \tag{4}$$

At the sediment layer boundary $z=H$, when the shear wave incidence angle from the sediment into water satisfies $\theta_2<\arccos(c_{s2}/c_1)$, the boundary satisfies total internal reflection with amplitude $|V_{s12}|=1$, and phase ϕ_{s12} [28]:

$$\phi_{s12}=-2\arctan\left(\frac{\rho_1 c_1^2}{\rho_2 c_{s2}^3}\sqrt{\frac{1-u^2/c_1^2}{u^2/c_{s2}^2-1}}\right) \tag{5}$$

Under the condition $c_{s2}<c_1<c_{p2}$, the $\arccos(c_1/c_{p2})$ is always less than $\arccos(c_{s2}/c_1)$, so the condition of total reflection at the upper boundary must be satisfied.

At the $z=H+h$ boundary, reflection between the sedimentary layer and basement can also be simplified to shear-wave-to-shear-wave reflection, because only shear waves propagate in the sedimentary layer within the $\theta<\arccos(c_1/c_{p2})$ range. In this case, the shear wave reflection coefficient at the lower boundary simplifies to

$$V_{s32}\big|_{\theta<\arccos(c_1/c_{p2})}=\frac{Z_{s3}\cos\theta_s-Z_{s2}\cos\theta_{s3}}{Z_{s3}\cos\theta_s+Z_{s2}\cos\theta_{s3}} \tag{6}$$

Where $Z_{s2}=\rho_2 c_{s2}$ and $Z_{s3}=\rho_3 c_{s3}$ are the shear wave impedances of the sediment medium and basement, respectively. According to Snell's law, when $c_{s3}>c_{s2}$ and the incident wave is at or above the critical angle, $\cos\theta_{s3}$ becomes purely imaginary, making reflection coefficient (6) complex, and total internal reflection occurs at the lower boundary. The lower boundary shear wave reflection coefficient can be expressed as $V_{s32}=\exp^{(i\phi_{s32})}$ with phase ϕ_{s32} [28] in the range of $\theta<\arccos(c_1/c_{p2})$:

$$\phi_{s32}=-2\arctan\left(\frac{\rho_3 c_{s3}^2}{\rho_2 c_{s2}^3}\sqrt{\frac{1-u^2/c_{s3}^2}{u^2/c_{s2}^2-1}}\right) \tag{7}$$

In the $H < z < H + h$ sediment layer, when the frequency corresponds to the cutoff frequency of a sediment shear wave mode, the shear wave horizontal wavenumber is $k_{s2} = k_1$, and the phase velocity is $u = c_1$, where $k_1 = \omega / c_1$ is the horizontal wavenumber in water. At this frequency, shear waves in the sediment layer experience total internal reflection at both upper and lower boundaries simultaneously, and acoustic energy is confined within and propagates along the sediment layer, manifesting as shear wave resonance. The $\phi_{s12} = 0$ can be found by substituting the phase velocity $u = c_1$ into the Eq. (5). Substituting the phases of both boundary reflection coefficients into Eq. (4) then gives the shear wave resonance frequency for the elastic sediment layer seabed:

$$f_n = \frac{c_{s2}}{2\pi h \sqrt{1 - c_{s2}^2 / c_1^2}} \left[\arctan\left(\frac{\rho_3 c_{s3}^2}{\rho_2 c_{s2}^2} \sqrt{\frac{1 - c_1^2 / c_{s3}^2}{c_1^2 / c_{s2}^2 - 1}} \right) + (n-1)\pi \right], \qquad n = 1, 2, 3 \cdots \tag{8}$$

The frequency interval between adjacent orders is

$$\Delta f = \frac{c_{s2}}{2h \sqrt{1 - c_{s2}^2 / c_1^2}} \tag{9}$$

The fundamental frequency (n=1) is

$$f_1 = \frac{c_{s2}}{2\pi h \sqrt{1 - c_{s2}^2 / c_1^2}} \arctan\left(\frac{\rho_3 c_{s3}^2}{\rho_2 c_{s2}^2} \sqrt{\frac{1 - c_1^2 / c_{s3}^2}{c_1^2 / c_{s2}^2 - 1}} \right) \tag{10}$$

The mathematical structure of the shear wave resonance frequency for elastic sediment layers is very similar to that for longitudinal wave resonance in soft sediment seabeds[10], but depends physically on the shear wave velocity.

Fig. 8 shows low-grazing-angle reflection loss at three angles (50-200 Hz) for the elastic sediment seabed parameters in Tab. 2, along with resonance frequencies of orders 4-10 calculated from the shear wave resonance frequency expression. The shear wave resonance frequencies are seen to align well with the frequencies of maximum low-grazing-angle reflection loss for the elastic sediment, effectively revealing the relationship between shear wave resonance and elastic sediment low-grazing-angle reflection characteristics.

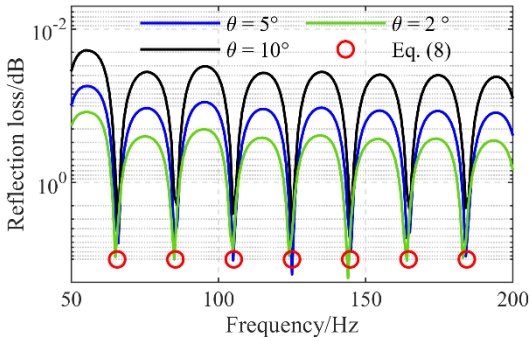

Figure 8. Frequency relationship between low grazing angle reflection and shear wave resonance in elastic seabed. The green, blue, and black curves represent the reflection loss curves for grazing angles of 2 °, 5 °, and 10 °, respectively; the red circle is the shear wave resonance frequency (Eq. (8)).

Table 2. Acoustic parameters of elastic sediment seabed.

Acoustic parameter	Compressional wave speed($m \cdot s^{-1}$)	Shear wave speed($m \cdot s^{-1}$)	Thickness (m)	Density/ ($g \cdot cm^{-3}$)	Compressional wave attenuation($dB \cdot \lambda^{-1}$)	Shear wave attenuation ($dB \cdot \lambda^{-1}$)
Water	1499	—	100	1.0	0.0	—
Sedimentary	1600	700	15	1.6	0.1	0.1
Basement	2800	1600	—	2.2	0.2	0.2

3.3 Acoustic Propagation Characteristics of Elastic Sediment Seabed

Shear wave resonance induced by low-grazing-angle reflection from elastic sediment bottoms can significantly affect acoustic propagation in water. Using the normal mode model KRAKENC[26], propagation loss in the frequency-distance domain is calculated for the same environments as in Fig. 7, as shown in the Fig. 9. Fig. 9(a) shows that propagation loss in low-sound-speed fluid seabed environments increases anomalously at frequencies corresponding to maximum small-grazing-angle reflection loss, with the high propagation loss features being more pronounced at higher frequencies and longer ranges. Because shear waves in elastic sediment layers similarly modulate low-grazing-angle reflection, manifested as shear wave resonance in the sediment layer, the propagation loss exhibits similar frequency characteristics to that in low-sound-speed fluid seabeds, but with smaller frequency intervals (Fig. 9(b)). Note that the frequency characteristics for both low-sound-speed fluid and elastic sediment seabeds differ significantly from the typical range-frequency interference structure of high-sound-speed seabeds (Fig. 9(c)), indicating that low-grazing-angle reflection characteristics significantly affect long-range acoustic propagation, and confirming that the $\Delta f \approx 26$Hz acoustic siphon effect observed in the experiment is related to low-grazing-angle reflection from the elastic seabed.

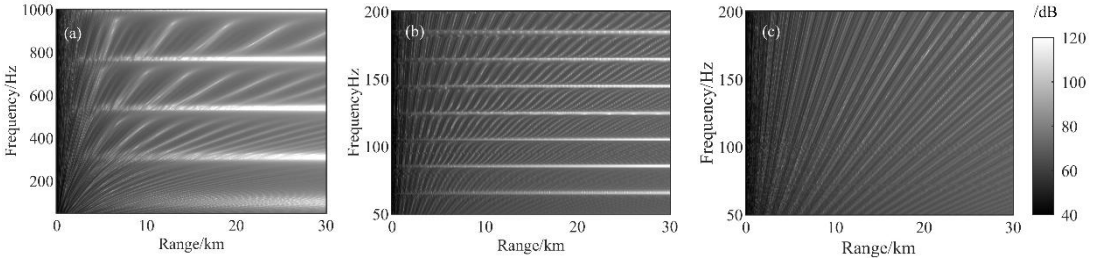

Figure 9. Frequency characteristics of propagation loss, where the sound source depth is 50 m, and the receiving depth is 80 m: (a) Low-velocity sediment seabed; (b) the elastic sedimentary seabed; (c) the high-velocity liquid seabed.

Combining Fig. 8 and Fig. 9(b), note that the shear wave resonance frequency for elastic sediment layers is derived under low-grazing-angle conditions, thus the elastic seabed shear wave resonance frequencies correspond to low-grazing-angle reflection characteristic frequencies. Simultaneously, when seabed resonance occurs, acoustic energy at the corresponding frequency leaks from the water into the seabed, causing abnormally high propagation loss in water at that frequency, i.e., the acoustic siphon effect.

4. Inversion of elastic bottom acoustic parameters

To verify the mechanism by which the elastic sediment layer geoacoustic model produces the observed acoustic phenomena, it is necessary to effectively invert the seabed parameters of the experimental environment. The difficulties in the inversion of acoustic parameters of elastic sediments are as follows: 1) the inversion parameters involve the combination of multi-dimensional parameters; 2) There is an obvious coupling effect among the parameters, which makes it difficult to obtain the optimal inversion results. In order to obtain the optimal inversion results, the parameters related to the acoustic characteristics concerned in this paper are analyzed by using the expression of shear wave resonance frequency.

4.1 Analysis of shear wave resonance frequency parameter

4.1.1 Sensitivity of shear wave resonance frequency to sound attenuation

Seabed acoustic attenuation is a key parameter affecting long-range acoustic propagation in shallow water, analyzing the sensitivity of shear wave resonance frequency to acoustic attenuation is important for effectively determining seabed parameters. From Fig. 8, the frequencies of maximum low-grazing-angle reflection loss correspond to shear wave resonance frequencies for elastic sedimentary bottoms. Fig.10(a) shows reflection loss versus sediment shear wave attenuation for five resonance frequencies (n=9, 11, 14, 16, 18). Different-order resonance frequencies are similarly affected by sediment shear wave attenuation, with the maximum

low-grazing-angle reflection loss first increasing then decreasing as sediment shear wave attenuation increases, and lower frequencies exhibiting maximum reflection loss at higher attenuation coefficients.

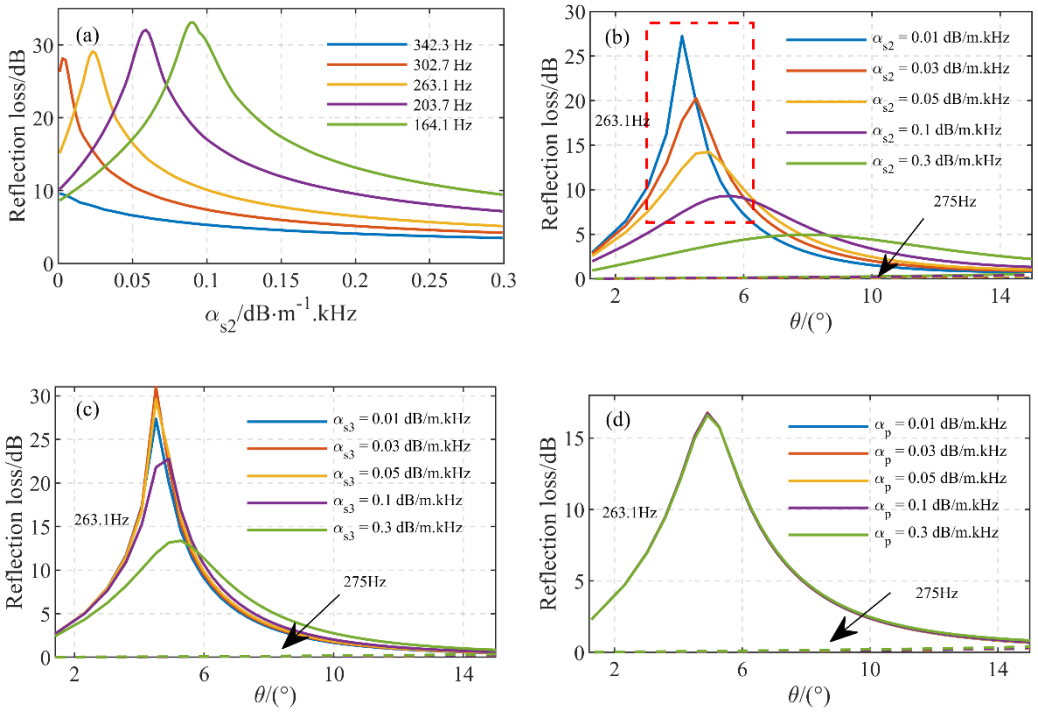

Figure 10. Sensitivity analysis of low grazing angle reflection loss characteristics of shear wave resonance frequency: (a) Relationship between bottom reflection loss and shear wave attenuation, and the maximum reflection loss of low grazing angle ($\theta < \arccos\left(c_1/c_{p2}\right)$) **(**is taken in the same environment; (b) sensitivity of the resonance frequency 263.1 Hz to the shear wave attenuation: (c) sensitivity of the resonance frequency 263.1 Hz to the base shear wave attenuation; (d) sensitivity of the resonance frequency 263.1 Hz to the longitudinal wave attenuation.

Taking the resonant frequency of 263. 1 Hz as an example, the effects of acoustic attenuation of shear wave in the sedimentary layer, acoustic attenuation of shear wave in the basement, and attenuation of longitudinal wave on the maximum peak of reflection loss at low grazing angle are analyzed. By analyzing Fig. 10(b)~(d), it can be seen that the maximum peak of reflection loss at low grazing angle is very sensitive to the attenuation of shear wave in the sedimentary layer, followed by the attenuation of shear wave in the basement, and the attenuation of longitudinal wave hardly affects the reflection at low grazing angle. Moreover, the reflection loss at non-resonant frequencies is not sensitive to shear wave attenuation, such as the low grazing angle reflection loss curve at 275 Hz in Fig. 10(b)~(d). The results effectively reflect the influence of acoustic attenuation on the low grazing reflection and resonance frequency of the elastic sediment.

4.1.2 Parameter coupling analysis

Besides acoustic attenuation, various geoacoustic parameters related to elastic seabed shear wave resonance frequency also affect the corresponding acoustic propagation characteristics. To analyze parameter coupling relationships, the following cost function is constructed to examine coupling in seabed shear wave resonance frequency characteristics.

$$E(\mathbf{n}) = \frac{1}{\sqrt{\left(f_{1c}(\mathbf{n}) - f_{1e}\right)^2}} \tag{11}$$

Where f_{1c} represents the theoretically calculated fundamental frequency, f_{1e} is the experimentally measured fundamental frequency, and $\mathbf{n}$ is the inversion parameter vector. Fig. 11 shows logarithmic two-dimensional cost function results for parameters related to shear wave resonance fundamental frequency versus shear wave velocity, where true values correspond to red box positions. The cost function reaches maximum at true values, but significant coupling exists among the acoustic parameters. Sediment layer thickness and density are positively correlated with sediment shear wave velocity, while basement shear wave velocity is negatively correlated with sediment shear wave velocity. Coupling between sediment layer shear wave speed and thickness is strongest, and parameter sensitivity to sediment shear waves satisfies $h > c_{s2} > c_{s3} > \rho_2 > \rho_3$. Therefore, although parameter combinations satisfying the fundamental frequency condition can be obtained through inversion using Eq. (11), correct optimal inversion results may not be obtained due to parameter coupling.

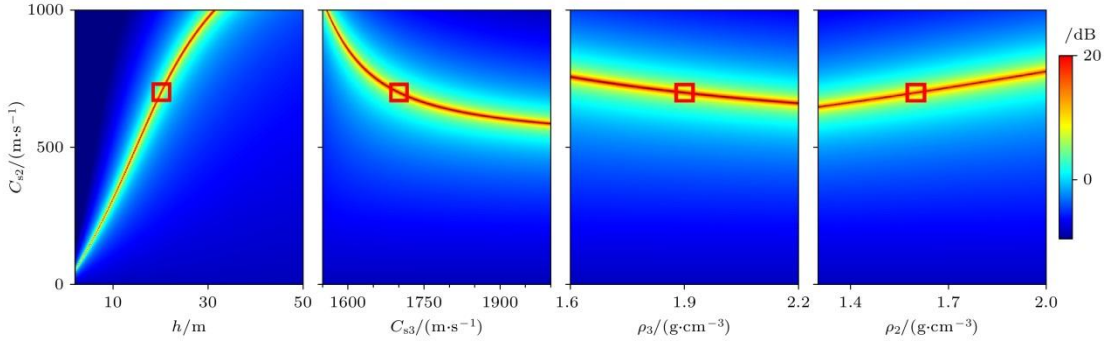

Figure 11. Coupling relationship of shear wave resonance frequency: closed-form expression.

Due to OBS sensitivity to seabed vibration, measurement results from simultaneous seabed-waveguide acoustic propagation can help pre-determine optimization intervals for specific parameters. In our case, coupling between sediment shear wave velocity and thickness is strongest. Therefore, sediment shear wave velocity ranges can be pre-determined using acoustic vector signals measured by OBS, then constraining either shear wave speed or thickness ranges during elastic bottom parameter inversion, helps obtain optimal seabed acoustic parameters.

4.2 Inversion of elastic bottom parameters

4.2.1 Range of shear wave sound velocity

In the Dongsha joint seabed-waveguide acoustic propagation experiment, OBS measured seabed vibration velocity signals, enabling direct calculation of seabed acoustic signal pitch angles using the complex acoustic intensity method. Fig. 12 shows time-domain waveforms of horizontal and vertical particle velocity components received by OBS, and pitch angles for sources at different distances. The figure shows that at 19.82 km range, vertical component particle velocity amplitude received by OBS is significantly stronger than horizontal component[6,7], and acoustic signal pitch angles are relatively stable beyond 2 km horizontal distance, averaging 67.98 °. This indicates seabed shear wave velocity is lower than water sound speed, as Snell's law dictates that only when seabed shear wave velocity is less than water sound speed will vertically polarized shear waves excited in sediment by water-borne sources propagate at high grazing angles. Combined with previous analysis of elastic sediment seabed reflection loss characteristics, we know that shear wave resonance primarily arises from low-grazing-angle reflection. Therefore, sediment shear wave velocity can be determined to range between 562.27 m/s and 800 m/s, providing an effective optimization range for subsequent inversion of seabed sediment shear wave velocity, and partially avoiding strong coupling between sediment shear wave speed and other parameters.

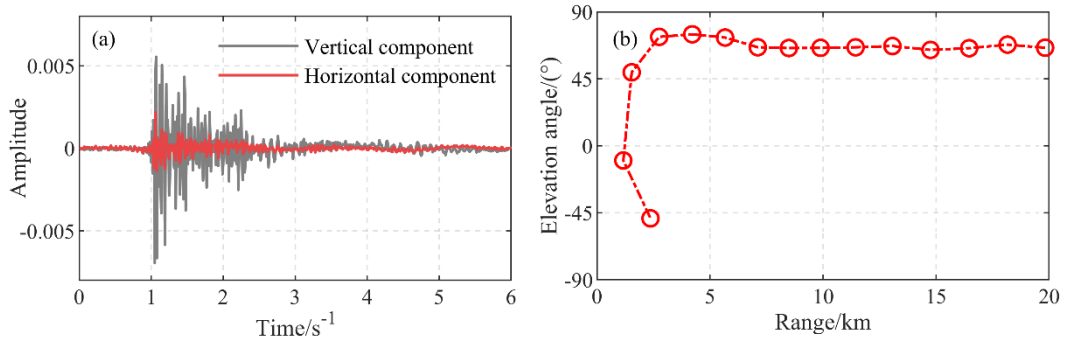

Figure 12. (a) Time domain waveforms of the horizontal and vertical components of the particle velocity signal received by the OBS. The sound source is 19.82 km away from the OBS; (b) the elevation angle of the 0–20 km sound source is calculated by using the complex sound intensity method.

4.2.2 Inversion strategy

Under simultaneous seabed-waveguide measurement conditions, frequency siphons and seabed resonance from broadband sources in water can be observed simultaneously. Based on acoustic siphon characteristics observed in water, seabeds can be classified as low-sound-speed sediment seabeds or elastic sediment seabeds, and initial siphon frequency and frequency interval can be calculated. If acoustic siphon or seabed resonance frequency intervals are small, the seabed environment is identified as elastic sedimentary. Then, using measured resonance frequency

intervals, the relationship between sediment shear wave velocity and thickness can be determined. Simultaneously, seabed acoustic signal pitch angles (grazing angles) can be calculated from OBS vibration velocity signals. Snell's law provides the relationship between sediment shear wave velocity and grazing angle of acoustic waves transmitted from water to seabed. Under these constraints, an incoherent Bartlett processor is used to construct a matching cost function, and the particle swarm optimization global search algorithm[29] obtains optimal solutions, yielding optimal multi-dimensional geoacoustic parameter combinations for elastic sediment seabeds. The specific process is shown in Fig. 13.

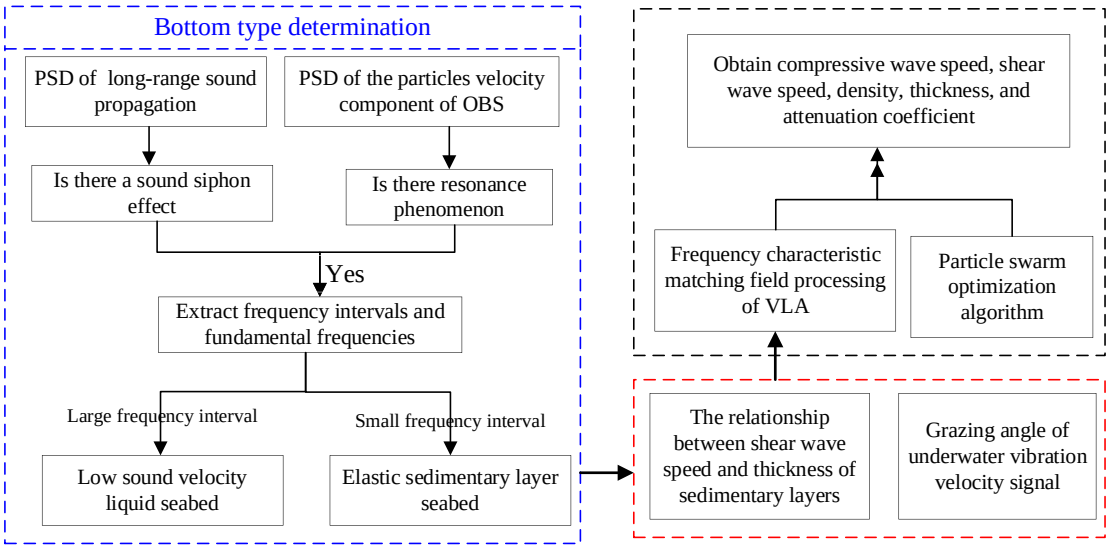

Figure 13. Inversion strategy.

Based on VLA received signal broadband characteristics, the matching cost function using the incoherent Bartlett processor is[16].

$$E(\mathbf{m}) = \frac{1}{M}\sum_{j}^{M}\left(\frac{\left|\sum_{i}^{N} p_i^{e}(f_j)^{*}\, p_i^{c}(f_j,\mathbf{m})\right|^2}{\left[\sum_{i}^{N}\left|p_i^{e}(f_j)\right|^2\right]\left[\sum_{i}^{N}\left|p_i^{c}(f_j,\mathbf{m})\right|^2\right]}\right) \tag{12}$$

Where $p_i^{e}(f_j)$ represents sound pressure measured by the i vertical array element; $p_i^{c}(f_j,\mathbf{m})$ is the replica field of the i element calculated based on the normal mode theory, $\mathbf{m}$ represents the parameter vector to be inverted, j indexes frequency point, and Nis the number of vertical array elements 32; the M represents the number of frequency points used for inversion; The superscript "*" indicates conjugation.

Fig. 14 shows sensitivity of cost function $E(\mathbf{m})$ to elastic sedimentary seabed parameters in the actual waveguide environment. Within the ranges shown for eight geoacoustic parameters, sensitivities differ significantly, with sediment layer compressional wave velocity, shear wave

velocity, and thickness being most sensitive, while attenuation coefficients and densities are less sensitive. However, maxima occur at true values with no false peaks, avoiding local optimum traps and proving objective function feasibility. Section 4.1 shows shear wave resonance frequency is highly sensitive to acoustic attenuation, but in actual waveguide environment inversion, because Eq. (12) uses only single-source signals and is normalized, acoustic attenuation coefficient sensitivity is weak. Note that this paper focuses on how seabed geoacoustic models modulate seabed resonance and acoustic siphon characteristics, thus parameters obtained from Eq. (12) inversion do not affect our qualitative analysis.

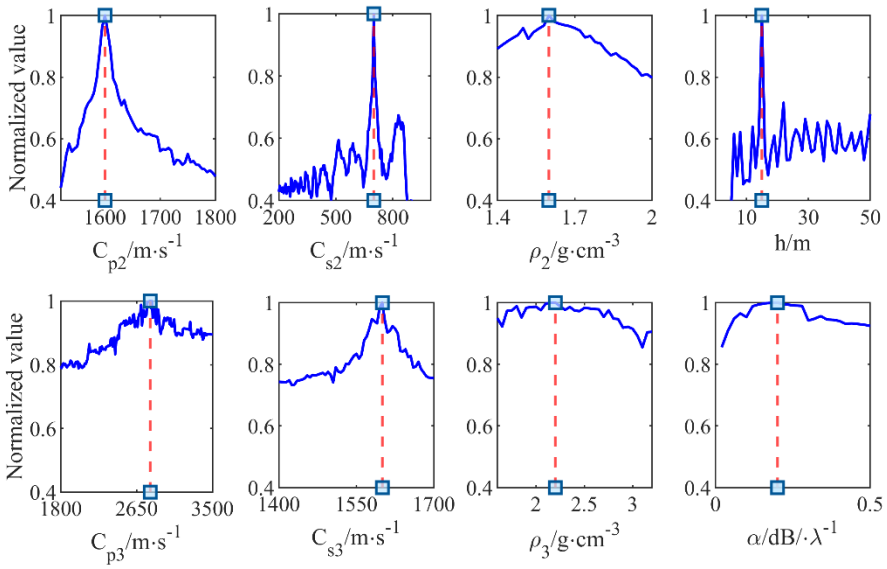

Figure 14. Sensitivity analysis of seabed parameters of elastic sediment layer in actual waveguide environment, the red dotted line is the true value.

4.2.3 Inversion result and characteristic verification

Following the inversion strategy in Fig. 13, seabed parameters in the experimental area were inverted. For inversion, three broadband explosive signals in the 100-180 Hz band (81 frequency points) were selected as measurement data. For particle swarm optimization, 80 particles were used with maximum iterations $t_{\max}=100$, with inertia weight decreasing as $w=0.9-(0.9-0.3)\cdot t/t_{\max}$, where t is iteration number. Learning factors also vary with iteration: $a_1=2.5-(2.5-0.5)\cdot t/t_{\max}$, $a_2=0.5-(0.5-2.5)\cdot t/t_{\max}$.

Table 3. Inversion results of seafloor geoacoustic parameters of the elastic sedimentary layer.

Layer	Inversion parameter	Search interval	Inversion result
Sedimentary layer	cp2/(m·s−1)	1550—1800	1640.7
	cs2/(m·s−1)	500—800	681.0
	h/m	2—40	14.5
	ρ2/(g·cm−3)	1.55—2.1	1.65

Layer	Inversion parameter	Search interval	Inversion result
	αp2/(dB·λ−1)	0.05—0.5	0.14
	αs2/(dB·λ−1)	0.05—0.5	0.11
Basement	cp3/(m·s−1)	1850—3000	2476
	cs3/(m·s−1)	1510—1800	1757.6
	ρ3/(g·cm−3)	2.15—4.0	3.5
	αp3/(dB·λ−1)	0.1—0.6	0.22
	αs3/(dB·λ−1)	0.1—0.6	0.29

Inversion results and optimization intervals are listed in Tab. 3. Substituting inversion results into Eqs. (9) and (10) yields resonance frequency interval 26.36 Hz and fundamental frequency 11 Hz, matching well with experimental siphon interval (~26 Hz) and OBS-observed resonance fundamental frequency (11.8 Hz). Using normal mode theory, 50-250 Hz propagation loss in the inversion environment was calculated, and shear wave resonance frequencies from Eq. (8) with inversion parameters were compared with measurements at two distances, as shown in Fig. 15. In the 50-250 Hz band, both inversion calculations and measured transmission loss show regular acoustic siphon characteristics, with measurements agreeing well with theoretical simulations. Acoustic siphon frequencies also agree well with shear wave resonance frequencies. These results verify both the reliability of seabed parameter inversion and that small-spacing acoustic siphon effects are caused by elastic sediment bottoms, and reveal the mechanism whereby shear-wave-modulated low-grazing-angle reflection confines acoustic energy in the seabed.

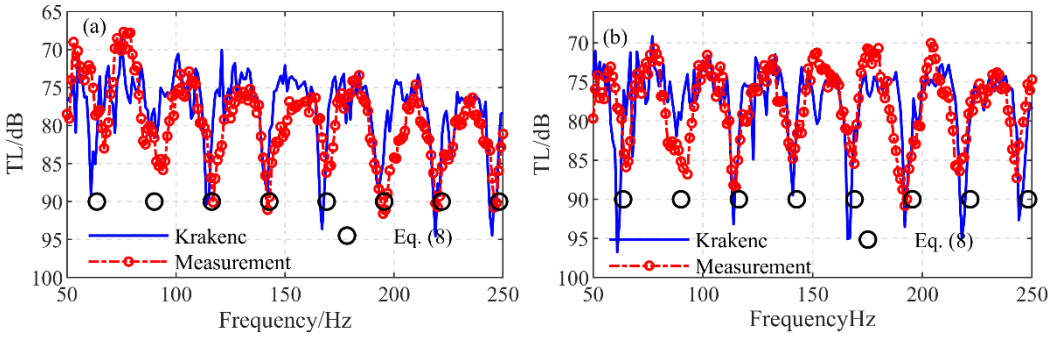

Figure 15. Propagation loss in the 50–250 Hz band calculated from the inversion results is compared with the experimental measurement: (a) Distance from a sound source to VLA is 20.8 km; (b) from the sound source to VLA is 24.99 km.

5. Conclusion

This paper studied low-grazing-angle reflection and shear wave resonance on elastic sediment bottoms using seabed and waveguide sound propagation data from the South China Sea Dongsha area. First, differences between frequency intervals of observed seabed resonance (or acoustic siphon) phenomena and those associated with low-sound-speed bottoms were analyzed, and shear wave resonance frequency theory for elastic sediment bottoms was derived under low-grazing-angle conditions, and effects of bottom environment on long-range shallow water acoustic propagation were examined. Results show that maximum low-grazing-angle reflection loss on elastic sediment seabeds provides the physical basis for seabed shear wave resonance, and that elastic sediment shear wave resonance causes confinement of water-borne acoustic energy in the sediment, thus causing abnormally high long-range acoustic transmission loss in shallow water. The relationship between seabed resonance and underwater acoustic siphon phenomena is effectively verified theoretically and experimentally.

Building on this, by analyzing sensitivity of shear wave resonance frequency to acoustic attenuation and parameter coupling relationships, a geoacoustic parameter inversion method combining seabed and waveguide observations is proposed. This method determines seabed type from long-range shallow water acoustic propagation frequency characteristics, determines sediment layer shear wave velocity range from OBS three-component vibration velocity signals, and finally obtains elastic seabed parameters by combining with traditional seabed parameter inversion approaches. Inversion results effectively verify that the experimental seabed is an elastic sedimentary seabed, and that shear-wave-modulated low-grazing-angle reflection from elastic sedimentary seabeds confines acoustic energy in the seabed.

Acknowledgments

We thank all participants in the summer 2021 South China Sea Dongsha underwater acoustic experiment, whose hard work provided reliable experimental data for this paper.

References

[1] Katsnelson B, Petnikov V, Lynch J 2012 *Fundamentals of Shallow Water Acoustics* （New York: Springer Press） p65

[2] Duncan A J, Gavrilov A N, McCauley R D, Parnum I M, Collis J M 2013 *J. Acoust. Soc. Am.* **134** 207

[3] Godin O A 2021 *J. Acoust. Soc. Am.* **149** 3586

[4] Godin O A 2025 *J. Acoust. Soc. Am.* **157** 314

[5] Zhang S Z, Piao S C 2021 *Acta Phys. Sin.* **70** 214304

[6] Akal T, Berkson J 1986 *Ocean Seismo-Acoustics: Low-Frequency Underwater Acoustic* （New York & London: Nato Scientific Affairs Division Plenum Press） p149

[7] Xie J H, Cao D J, Zhang H G 2024 *Journal of Physics: Conference Series 2718* Changsha City, China, October 13–15, 2023 p012070

[8] Fokina M S, Fokin V N 2001 *J. Comput. Acoust.* **09** 1079

[9] Godin O A, Chapman D M F 1999 *J. Acoust. Soc. Am.* **106** 2367

[10] Godin O A, Deal T J, Dong H F 2021 *J Acoust Soc Am.* **149** 49

[11] Dall'Osto D R, Tang D J 2022 *J. Acoust. Soc. Am.* **151** 3473

[12] Hastrup O F 1980 *Some Bottom-Reflection Loss Anomalies near Grazing and Their Effect on Propagation in Shallow Water" In Bottom-Interacting Ocean Acoustics* edited by Kuperman W A, Jensen F B （New York: Plenum Press） p135

[13] Hermand J P, Siderius M 1997 *J. Acoust. Soc. Am.* **102** 3142

[14] Wilson P S, Knobles D P, Neilsen T B 2020 *IEEE J. Ocean. Eng.* **45** 1

[15] Wilson P S, Knobles D P, Neilsen T B 2022 *IEEE J. Oceanic Eng.* **47** 497

[16] Zhou J X, Li Z L, Zhang X Z, Qin J X 2024 *J. Acoust. Soc. Am.* **155** 3490

[17] Li M Z, Li Z L, Zhou J X, Zhang R H 2019 *Acta Phys. Sin.* **68** 094301

[18] Zhou J X, Qin J X, Li Z L, Zhang X Z 2024 *J. Acoust. Soc. Am.* **156** 1575

[19] Hughes S J, Ellis D D, Chapman D M F, Philip R S 1990 *J. Acoust. Soc. Am.* **88** 283

[20] Hovem J M, Solberg C E, Tollefsen D 2001 *Annual Conference of the Marine-Technology-Society* Honolulu, HI, USA, November 5–8, 2001 p715

[21] Zhang H G, Xie J H, Wang X H, Ma Z K 2024 *Acta Acustica* **49** 835

[22] Zheng G X, Piao S C, Dong Y, Gong L J 2024 *JASA Express Lett.* **4** 126004

[23] Li L, Chen Z, Liu J G, Chen H, Yan W, Zhong Y 2014 *J. Trop. Oceanogr.* **33** 54

[24] Vanneste M, Madshus C, Socco V L, Maraschini M, Sparrevik P M, Westerdahl H, Duffaut K, Skomedal E, Bjørnara T I 2011 *Geophys. J. Int.* **185** 221

[25] Socco V L, Boiero D, Maraschini M, Vanneste M, Madshus C, Westerdahl H, Duffaut K, Skomedal E 2011 *Geophys. J. Int.* **185** 237

[26] Acoustics toolbox, Porter M B https://oalib-acoustics.org/ [2025-5-20]

[27] Zhang R H, Li F H 1999 *Sci. China, Ser. A Math. Phys. Astron.* **42** 739

[28] Brekhovskikh L M, Godin O A 1998 *Acoustics of Layered Media. 1: Plane and Quasi-Plane Waves* （Vol. 2） （Berlin: Springer Press） p14

[29] Kennedy J, Eberhart R 1995 *IEEE Int Conf on Neural Networks* Perth, WA, Australia, November 26–December 2, 1995 p1941